C-CNN: Contourlet Convolutional Neural Networks

Mengkun Liu, Licheng Jiao, *Fellow, IEEE,* Xu Liu, *Member, IEEE,* Lingling Li, *Member, IEEE,* Fang Liu, *Senior Member, IEEE,* Shuyuan Yang, *Senior Member, IEEE*

***Abstract*—Extracting effective features is always a challenging problem for texture classification, since the uncertainty of scales and the clutter of textural patterns. For texture classification, spectral analysis is traditionally employed in the frequency domain. Recent researches have shown the potential of convolutional neural networks (CNN) when dealing with the texture classification task in the spatial domain. In this paper, we try combining both approaches in different domain for more abundant information, and proposed a novel network architecture named Contourlet CNN (C-CNN). The network aims to learn sparse and effective feature representations for images. First, the Contourlet transform is applied to get the spectral features from an image. Second, the spatial-spectral feature fusion strategy is designed to incorporate the spectral features into CNN architecture. Third, the statistical features are integrated into the network by the statistical feature fusion. Finally, the results are obtained by classifying the fusion features. We also investigated the behavior of the parameters in Contourlet decomposition. Experiments on the widely used three texture datasets (kth-tips2-b, DTD, and CUReT) and five remote sensing datasets (UCM, WHU-RS, AID, RSSCN7 and NWPU-RESISC45) demonstrate that the proposed approach outperforms several well-known classification methods in terms of classification accuracy with fewer trainable parameters.**

***Index Terms*—Multi-Scale, contourlet transform, texture classification, remote sensing scene classification.**

I. Introduction

TEXTURE is defined as smoothness or roughness of the surface of an object, which contains important information about the structural arrangement of surfaces and their relationship to the surrounding environment [1], such as the grain of the wood and the pattern of fabric with repeated structure. Texture is a key visual cue for various image analysis applications like image segmentation, image classification, and texture synthesis. It plays a significant role in biomedical image analysis, remote sensing, object recognition [2], etc. Texture classification, a process of assigning an unknown texture to a known set of texture class, has been an active research topic due to challenges about the uncertainty of scales, lighting conditions, the clutter of textural patterns, even textures within the same class can vary greatly.

Traditional texture classification generally consists of two main stages: feature extraction and classification. With the pioneering work of Juleszs [3], early texture feature extraction methods are based on statistics [1, 4, 5], geometry [6, 7], structure [8–12], model [13, 14] , transform in signal processing [15–18] and the multiresolution analysis [19–30]. In classification stage, the extracted features are then classified by various classifiers such as SVM [31–34], learning vector quantization (LVQ) [35], Bayes [36] and K-nearest-neighbor classifier (K-NN) [37–39].

A. Texture Feature Extraction

1) The statistics-based methods: The statistics-based methods provide measures of distribution properties of pixels intuitively. Such as gray-level co-occurrence matrices (GLCM) [1], which represent co-occurrences of the pixel intensities at given angles and distances. The gray-tone spatial-dependence matrices (GTSDM), based on statistics that summarize the relative frequency distribution [1], provide an efficient texture classification with two decision rules: a piecewise linear decision rule and a min-max decision rule. The similar work in [4] aimed to measure the statistical properties of pixel pairs at several distances with the statistical feature matrix, the major property that differs from [1] is the matrix size depends on the maximum distance rather than the number of gray-levels. The features such as the Fourier power spectrum, first-order statistics of gray level differences and second-order gray level statistics are extracted as texture representation [5].

2) The geometry-based methods: The geometry approaches represent textures with the properties of geometrical constraints. Blostein [6] integrates the texture elements with the corresponding scene layout, which identifies the texture elements and recovers the orientation of texture simultaneously by constructing a multi-scale region detector in a Laplacian-of-Gaussian scale-space. They overcame the challenges in practice that the texture is occluded partially or in fine scale. Stevens [7] proposed the valid constraints to compute surface orientation and distance via a visual analysis which uses the surface shape and contour of the texture. It can be decomposed into two modules: the contour generators reconstruction and the surface relation determination, which separates the problem of the projective geometry from the intrinsic geometry.

3) The structure-based methods: The structure-based methods find the local or global properties of textures with a specified descriptor. Traditional texture descriptors such as

This work was supported by the State Key Program of National Natural science of China (No.61836009), Project supported the Foundation for innovative Research Groups of the National Natural Science Foundation of China (No.61621005), the Major Research Plan of the National Natural ScienceFoundation of China (No.91438201, 91438103, 61801124), the National Natural Science Foundation of China(No.U1701267, 61871310, 61573267,61906150), the Fund for Foreign Scholars in University Research and Teaching Programsthe 111 Project(No. B07048),the Program for Cheung Kong Scholars and Innovative Research Team inUniversity(No.IRT 15R53), the S&T innovation project from Chinese Ministry of Education, the NationalScience Basic Research Plan in Shaanxi Province of China (No.2019JQ-659), and the China Postdoctoral Fund (No. 2019M663641). *(Corresponding author: Licheng Jiao.)*

The authors are with the Key Laboratory of Intelligent Perception and Image Understanding of Ministry of Education, International Research Center for Intelligent Perception and Computation, Joint International Research Laboratory of Intelligent Perception and Computation, SchoolofArtificialIntelligence, Xidian University, Xian, Shaanxi Province 710071, China (e-mail: lchjiao@mail.xidian.edu.cn; mengkunliu31@163.com).

local binary patterns (LBP) [8] and its extensions [10–12] are used for capturing the main properties of the texture. The LBP describes the texture as a two-level version of the texture spectrum [9]. The complementary information for effective texture representation is provided by a simple contrast measure [10], but it is still rotation variant. Later, Ojala [11] improved the LBP further with multi-resolution gray-scale and rotation invariant. The completed robust local binary pattern (CRLBP) has been developed for improving the robustness to noise and illumination variants [12]. The volume local binary pattern (VLBP) is proposed as a dynamic texture descriptor in the temporal domain, combining motion and appearance. The completed local binary pattern (CLBP) [37] can effectively represent the missing information in the LBP with center pixel and a local difference sign-magnitude transform. These methods describe the local or global properties of textures, but it is difficult to study the heredity or dependence of pixels between texture scales.

4) The model-based methods: The model-based methods describe texture with estimated parameters of the model. It is under the hypothesis that texture is formed on a distributed model with the interaction of correlated random variables in spatial domain. Common model-based approaches include Gaussian Markov random field model [13], simultaneous autoregressive model [14], random field model [40, 41], fractal model [42] and so on, whereas the computation burden is significantly increased when the model is complex.

5) The signal processing-based methods: The traditional feature extraction methods in signal processing also achieved satisfactory results. Bovik [15] measured the local values of the fractal dimension by multiple Gabor filters. The spatial frequency filter and the orientation channel filter are introduced to texture analysis [16]. The multi-scale Hurst parameters are used as features for texture classification, which is comparable with Gabor features [17]. The rotation-invariant texture features are generated via the circular neighborhoods and 1-D discrete Fourier transforms [18].

6) The multiresolution analysis-based methods: Instead of describing the texture features in the former case, the multiresolution analysis-based approaches describe the energy distribution in the spectral domain. It can efficiently capture the intrinsic geometrical structures of texture. In addition, more precise texture information is obtained by compact energies. The multiscale transforms mainly include the wavelet transform [19, 31, 34, 39], the shearlet transform [20–22], the ridgelet transform [23], the curvelet transform [24], the contourlet transform [25–27] and the brushlet transform [28–30], the multi-resolution and orientated representations of these transforms are suitable to describe texture with repeated structure.

B. Texture classification

Traditional methods performs well in classification such as SVM [31–34, 43] and K-nearest-neighbor classifier (K-NN) [37–39]. However, the extracted handcrafted features of the involved algorithms rely heavily on the experience, and the classifier is separated from feature extraction in two stages. In recent years, CNN has achieved remarkable results in many fields as an end-to-end method [44–54].

With the recent researches on deep learning [55, 56], convolutional neural networks (CNN), a biologically inspired multistage structure, has enjoyed significant performance on some tasks such as image classification [57], semantic segmentation [58, 59] and object detection [60]. It utilizes the features extracted by networks directly rather than carefully designed. The methods based on CNN are considerably better than the previous state-of-the-art methods.

CNN is first introduced in texture classification where feature extraction and classification are processed in the same four layer network [61]. Later, CNN is applied to lung image classification [44] and forest species recognition [45] in 2014 since both tasks can be viewed as the texture classification problems. However, these approaches are not specifically tailored for textures.

For texture classification, CNNs cannot be handled very well. The reason is that the repeated patterns have lower complexity in texture, while CNN is appropriate to extract high-level semantic features. Besides, parameters and computational complexity is greatly increased. Under such circumstance, the improved texture classification on CNN is specifically addressed in an end-to-end fashion. In [46–49], network architectures are modified by considering texture characteristics. FV-CNN [46], a valid texture descriptor, is obtained by Fisher Vector pooling of a CNN filter bank. Texture CNN (T-CNN) is developed [47] on AlexNet with an energy measure, namely, a new energy layer is derived from the last convolution layer by averaging the output in each feature map. It is similar to an energy response of a filter bank. The approach improved classification accuracy slightly while reduced complexity with fewer parameters. Wavelet CNN [48], [49] is proposed to integrate the haar wavelet decomposition as a spectral analysis into CNN. Based on the insight that the pooling and the convolution can be thought as a limited form of spectral analysis, thus it captures both types of features well under a single model. Wavelet CNN [49] uses projection shortcuts [50] to maximize the retention of information flowing over the network, and dense connection [51] is applied for adapting changes to dimensions. Similar to the energy layer in T-CNN, global average pooling [52] is used rather than fully connected layer in order to prevent overfitting. Wavelet CNN achieves better accuracy with fewer parameters than CNNs, but unable to outperform Fisher Vector-CNN (FV-CNN) [46].

From the above CNN-based methods for texture classification, three main challenges can be summarized as follows.

1) Texture images usually include the local or global properties of uncertainty scales and various patterns. Feature representation within a fixed scale may not be robust and discriminative. Thus it's vital to study the heredity or dependence of pixels between texture scales.
2) In addition to spatial information, texture image contains rich spectral information. Therefore, how to mine and make full use of both information will be very helpful to the effective representation and classification.
3) High-level semantic feature extracted by CNN is not

appropriate for texture representation, since the repeated patterns in texture have lower complexity. Moreover, the computation burden is significantly increased when the model is complex.

C. Motivation

The image classification is to identify which class a given sample belongs to. The CNN-based classifier is employed in the proposed method. Given an input signal $x(u)$, $u \in \mathbb{R}^n$, with n=2 for images, a general convolutional network function in the specific layer x_j is defined as

$$\begin{aligned} x_j &= \rho W_j x_{j-1} \\ &= \rho \sum_k w_{j,k_j}(k) * x_{j-1}(k), \end{aligned} \tag{1}$$

where $j(0 < j \leq J)$ is the network depth, W_j is a linear operator which includes the bias for more concise expression. ρ denotes the nonlinearity transforms such as sigmoid or relu. k_j represents a channel index. The symbol $*$ is the convolution operator.

For most classification architectures, the W_j is covariant to translations. Data augmentation and deep architecture are common tricks to provide the geometric transformations. The pooling operation can keep consistent expression to small translation. Nevertheless, CNNs lacks the ability of geometric transformation to some extent.

In order to solve the above-mentioned problems, the Contourlet CNNs (C-CNN) is proposed in this paper, which is inspired by [49] and employs wavelet as a spectral analysis into CNN. Contourlet transform is a kind of multiscale geometric analysis tools and has the substantial advantages of locality and directionality. It can be introduced into neural network to enhance the ability of geometric transformations. Meanwhile, it avoids the network falling into the local optimum too early. The introduction of multi-scale geometric filter banks increase the interpretability and controllability of the network, which enhance the robustness of the scale and directionality.

Compared with the wavelet transform, the contourlet transform offers the better directionality, anisotropy, spatial locality and the bandpass property, which is consistent with the main characteristics of Human Visual System (HVS) [see Section II-*A*]. It can effectively capture the geometry of contours with the edge singularity features, whereas wavelet captures point singularity features [53]. Thus the contourlet transform has more sparse representation. The details concerning the sparsity comparison are shown in Section II-*A*. In addition, wavelet transform has limited directionality which only captures horizontal, vertical, and diagonal details. However, contourlet transform is a new extension to the wavelet transform, and provides more abundant directional information of texture. Therefore, the C-CNN based on contourlet transform [54, 62] and CNN provides multidirectional and multiscale information effectively. The proposed method mainly focuses on three aspects:

- *Obtaining Spectral Features From Different Scales:* We define layers to perform multi-resolution analysis by contourlet transform in the CNN framework, which allows forward propagation to learn more effective texture features. The role of prior knowledge and higher quality information are dominant in effective texture representation with multi-scale and multi-direction from contourlet transform. The information in both spatial and spectral domains can improve the approximation ability of the network, which is conducive to escaping from saddle point in network optimization.
- *Enhancing Features Representation:* In order to use the spectral features adequately and represent features effectively, the multi-feature fusion strategies are used in the framework.
- *Light Weight Structure:* Due to the tight frame with sparse factor of contourlet and simple backbone network, C-CNN achieves comparable accuracy with few trainable parameters. Besides, some weights in contourlet kernel can be interpreted to make the network from black box to grey box.

Fig. 2 presents an overview of the C-CNN. It combines spectral analysis by contourlet transform with CNN. To summarize, the main contributions of this paper are as follows:

1) A novel network architecture, named C-CNN, is proposed that combines the information in the spectral domain and the spatial domain.
2) The Contourlet transform is integrated into CNN in order to mine features in spectral domain and make the network more compact.
3) Multi-feature fusion strategies are designed to obtain better features, which include spatial-spectral feature fusion and statistical feature fusion.
4) We analyzed the sparsity theoretically of Contourlet and the parameters of Contourlet decomposition in C-CNN.

The remainder of this paper is organized as follows. Section II describes the proposed CNN-based network. Experiments and results discussion is presented in Section III. Section IV summarizes our work.

II. Contourlet Convolutional Neural Networks

For texture classification, it's vital for effective texture representation against the challenges that the uncertainty of scales and the clutter of textural patterns. Subsection *A* explains why the contourlet transform is a sparse representation rather than wavelet. Subsection *B* describes contourlet transform combined with CNN and feature representations in a multi-scale and multi-direction way. The implementation details of the proposed method are given in Subsection *C*.

A. A Sparsity of Contourlet

The receptive fields of the visual cortex in mammals can be characterized as being localized, oriented and band-pass [55], which are similar to the basis functions of contourlet transforms. The characters of the receptive fields enable the human visual system to "capture" key information in natural scenes with the least number of visual neurons, comparable to the most sparse representation of natural scenes [63].

According to the research results of physiologists on the Human Visual System (HVS) and the statistical model of natural images, the "optimal" image representation method should have the following characteristics [64]:

1) *Multi-resolution:* The image can be approximated continuously from coarse to fine resolution, which is equivalent to "band-pass".
2) *Locality:* The representation basis should be local in both spatial and spectral domains.
3) *Directionality:* The basis should be directional and not limited to three directions of the separable two dimensional wavelets.

Fig. 1 illustrates the representations of approximating curves with wavelet and contourlet. The wavelet approximate curves by point, and the basis of wavelet has square support intervals of different sizes at different resolutions. The number of non-zero wavelet coefficients increases exponentially when the scale becomes finer, and a large number of non-negligible coefficients appeared, thus the curve cannot be "sparsely" expressed.

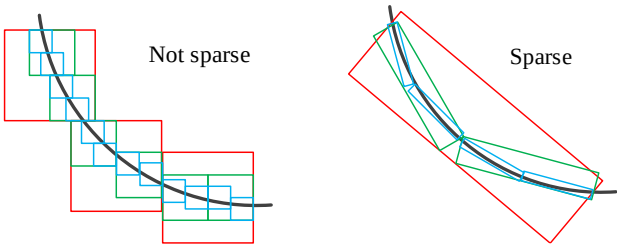

(a) Wavelet (b) Contourlet

Fig. 1. Comparison of the contour representations with the Wavelet and the Contourlet. (a) Wavelet has square supports that can only capture point discontinuities. (b) Contourlet has elongated supports that can capture linear segments of contours, and thus can effectively represent a smooth contour with fewer coefficients.

As one of the signal representation tools, contourlet is similar to the edge in object natural image. It can make full use of geometric regularity to obtain the sparse representation. Contourlet transform, an extension of wavelet transform, can describe a smooth contour as line segments with much fewer coefficients [see Fig. 1(b)]. However, there are largely inefficient decompositions as points in wavelet transform [see Fig. 1(a)]. Thus the representation of image with contourlet transform is more sparse since contours are basic units of image. The sparsity of contourlet is not limited to visual quality [see Fig. 1], but also in terms of the approximation rate. Next, we sketch briefly the approximation error and refer to [65] for details.

Given a 2-D piecewise smooth function f, which is C^2 (twice continuously differentiable) away from C^2 discontinuity curves. A general series expansion of f can be defined by:

$$f = \sum_{i=1}^{\infty} \alpha_i \phi_i, \tag{2}$$

with a basis $\{\phi_i\}_{i=1}^{\infty}$ such as Fourier or wavelet. The efficiency of an expansion can be measured by the nonlinear approximation (NLA) [66], which is defined as

$$\hat{f}_M^B = \sum_{i \in I_M} \alpha_i \phi_i, \tag{3}$$

where $\hat{f}_M^B$ is the best M-term approximation of function f with the basis B, and M is the number of the most significant coefficients. For the M-largest $|\alpha_i|$, I_M is the indexes of the M-term coefficients. $\hat{f}_M^B$ reflects the sparsity of the expansion by $\{\phi_i\}_{i=1}^{\infty}$. Thus the best M-term approximation error can be written as $\|f - \hat{f}_M^B\|_{L_2}^2$ in L_2-norm square. The M-term approximation error by contourlet frame satisfies

$$\|f - \hat{f}_M^{(contourlet)}\|_{L_2}^2 \leq C(logM)^3 M^{-2}. \tag{4}$$

Where C is a constant, the M-term approximation error of curvelet [67] is similar to contourlet, in order to compare the approximation performance of different basis concisely, the notation

$$A \asymp B \tag{5}$$

is introduced to mean the two expressions are equivalent within multiplicative constants. Namely, there are constants $C_1, C_2 > 0$ make $C_1 A \leq B \leq C_2 A$ valid. The squared error of M-term expansion with different basis satisfies:

$$\|f - \hat{f}_M^{(fourier)}\|_{L_2}^2 \asymp M^{-1/2} \tag{6}$$

$$\|f - \hat{f}_M^{(wavelet)}\|_{L_2}^2 \asymp M^{-1} \tag{7}$$

$$\|f - \hat{f}_M^{(contourlet)}\|_{L_2}^2 \asymp M^{-2} \tag{8}$$

The Eq.(6) and Eq.(7) show the decay rate of Fourier and wavelet are $O(M^{-1/2})$ [66] and $O(M^{-1})$ [53, 68], respectively. Contourlet has the decay rate of $O(M^{-2})$ in Eq.(8). The optimal approximation rate is M^{-2} according to reference [66]. In this case, the contourlet expansion can be seen as the optimal approximation rate. It compacts the signal f into a few coefficients and achieves the optimal sparse representation.

Moreover, the properties of directionality, localization, multiresolution and anisotropy that arise in contourlet proved strictly in reference [65]. Contourlet has elongated support intervals at various scales and directions with more sparse representation. Different directional contours in texture images can be described owing to an abundant directional selectivity. Therefore, contourlet should be a better choice than wavelet in feature representation of texture images.

B. Contourlet Convolutional Neural Networks Model

As a geometrical multiresolution analysis, the contourlet transform can efficiently represent texture image with basis of contours. It consists of an arbitrary number of directional bands at each level. The contourlet transform is formed by a tight frame with only a small redundancy factor. Therefore, we integrated the contourlet transform into CNN named Contourlet Neural Networks (C-CNN) [see Fig. 2], which can enhance the ability of feature representation, and improve the approximation ability of the network. Thus the Contourlet CNN provides a fast convergence speed with sparse and

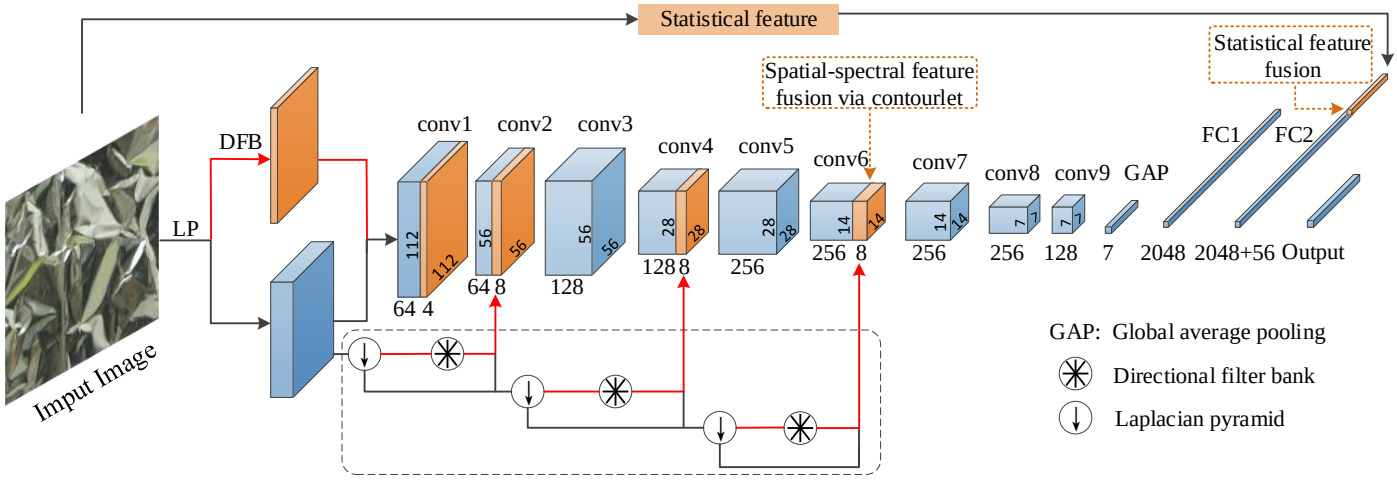

Fig. 2. C-CNN architecture. It includes three parts as follows. (a) Backbone: Mainly includes 9 convolution layers, 1 global average pooling layer followed by 3 fully-connected layers. (b) Multi-scale decomposition (in dotted box): the red line represents the flow direction of the high-frequency components, which are concatenated to corresponding feature maps in CNN with spatial-spectral feature fusion. (c) Statistical feature extraction: The mean and variance are calculated in each contourlet subband coefficient of the input image, and connected with FC2 to enhance feature representation and rotation invariant.

effective feature representation, and the better local optima is obtained.

In general, convolution layers in CNN can be denoted as $Y = (X * \mathbf{w})$, where X and Y are the input and output of the convolution layer, respectively. $\mathbf{w}$ represents the weights including the bias. The symbol $*$ is the convolution operator. Average pooling can be expressed as convolution by means of average filter and corresponding downsampling. Fujieda [49] considers CNN as parts of multiresolution analysis and represents convolution and pooling with a unified equation:

$$Y = (X * \mathbf{k}) \downarrow p \tag{9}$$

$$\mathbf{k} = \begin{cases} \mathbf{w} \; with \; p = 1, & convolution \\ \mathbf{p} \; with \; p > 1, & pooling \\ \mathbf{w} * \mathbf{p} \; with \; p > 1, & convolution + pooling \end{cases}$$

where $\mathbf{p}$ represents the averaging filter in pooling layers, and p is the stride of downsampling. Based on the equation (7) in [49], given an input X, the $X_{l,i}$ represents the low-pass component in level i thus $X_{l,0} = X$. The output of contourlet decomposition in level i can be described by the following equations:

$$\begin{aligned} X_{l,i+1}, X_{h,i+1} &= (X_{l,i} * F_{LP}) \downarrow p \\ X_{h\_bds,i+1} &= (X_{h,i+1} * F_{DFB}) \end{aligned} \tag{10}$$

Where F_{LP} and F_{DFB} are the laplacian pyramid and directional filter bank, respectively. p denotes the interlaced down sampling factor. The symbol $\downarrow$ is downsampling operator resembles the pooling operation in CNN. The subscript l, h of X represent the low-pass and high-pass component, respectively. The subscript h_bds denotes the bandpass directional subbands. CNN ignores the high-pass components. Therefore, the spectral information is integrated into CNN as shown in Fig. 2, where additional spectral information is highlighted and generated by the contourlet transform.

The well-trained filters in CNN with different orientations can capture edges in different directions in the spatial domain. Similarly, traditional filters such as contourlet filters have natural advantages for edge representation with different scales and directions in the spectral domain, which is neglected in CNN.

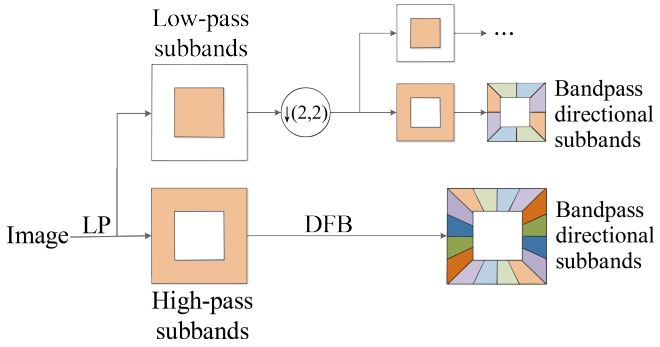

Fig. 3. Pyramidal directional filter bank of Contourlet decomposition. It is achieved by LP and DFB for low-pass subbands iteratively. The input image is first decomposed by LP filter to low-pass subbands and high-pass subbands, then the high-pass subbands are decomposed into 2^i directional subspaces through the DFB.

Fig. 3 shows the contourlet transform decomposed independently with multi-scale and multi-direction by iteratively adopting pyramidal directional filter bank (PDFB) on the low pass image. For example, the dotted box in Fig. 2 implements the three-levels contourlet decomposition by using PDFB iteratively. The PDFB is a cascade of a laplacian pyramid (LP) [69] and a directional filter bank (DFB) [70]. The input image is first decomposed by LP filter to low-pass subbands and high-pass subbands. The low-pass subbands are generated with two-dimensional low-pass analysis filtering and interlaced down sampling. The high-pass subbands are obtained by subtracting the low-pass component from the original image, where the low-pass component is the same size as the original image after applying up-sampling and low-pass synthesis filtering. High-pass subbands are decomposed

into 2^i directional subspaces through the directional filters (i is an arbitrary positive integer), then multi-resolution and multi-direction decomposition are achieved by performing the above steps on low-pass subbands iteratively. Thus abundant spectral information is obtained via contourlet transform from the original image.

The details of LP and DFB are shown in the following:

*1) **Laplacian pyramid**:* The laplacian pyramid (LP) is proposed to obtain multiscale decomposition by Burt and Adelson [69]. The LP decomposition at each level produces a low-pass component downsampled from the original signal and the residual signal between the original and the prediction, generating a band-pass component. Fig. 4 illustrates the decomposition process.

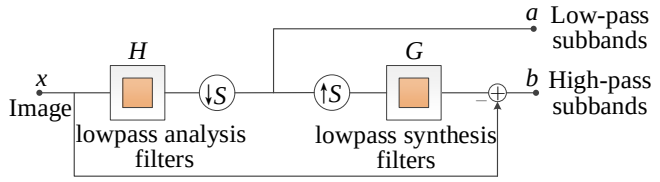

Fig. 4. One level of laplacian pyramid (LP) decomposition. First, the original image x is used to generate a downsampled low-pass subbands a through a lowpass analysis filters H and a sampling matrix S. The high-pass subbands b are then computed as the difference between the original x and the prediction with a sampling matrix S followed by a lowpass synthesis filters G.

Where H and G denote lowpass analysis and synthesis filters, respectively. $\boldsymbol{S}$ is called the sampling matrix. The decomposition can be iterated on the low-pass signal obtained by down-sampling. Sampling matrices are used in multidimensional filter banks. For instance, given the input signal x, the down-sampling version of signal x is obtained by an integer sampling matrix $\boldsymbol{S}$, resulting in $\boldsymbol{S}x$, the output a is a coarse approximation. b is a difference between the original signal and the prediction. Additionally, the effect that scrambled frequencies generated in the wavelet filter banks is avoided by only down sampling the low-pass channels.

*2) **Directional filter bank**:* Bamberger and Smith [70] introduced an oriented 2-D filter bank to reconstruct the original signal with a minimum sample representation. The directional filter bank (DFB) is generated by l-level binary tree decomposition in the two-dimensional frequency domain, resulting 2^l wedge-shaped subbands as shown in Fig. 5. The frequency domain is divided into $2^3 = 8$ directional sub-bands where l = 3, of which subbands 0-3 and 4-7 correspond to the vertical and horizontal details, respectively.

Minh N. Do [71] employed a 2^l parallel channel filter bank to represent a l-level binary tree with multirate identities. The parallel channel filter bank constructed from equivalent filters and sampling matrices. The equivalent filters are denoted by $G_k^{(l)}$, k is the subbands index as shown in Fig. 5 where $0 \leq k \leq 2^l$. Let $diag(a_1, \ldots, a_n)$ represent a diagonal matrix and a_n be the ith diagonal element. The corresponding sampling matrices are formed by:

$$\boldsymbol{S}_k^{(l)} = \begin{cases} diag(2^{l-1}, 2), & 0 \leq k \leq 2^{l-1} \\ diag(2, 2^{l-1}), & 2^{l-1} \leq k \leq 2^l \end{cases} \tag{11}$$

Given the discrete signal $y[\boldsymbol{n}]$ in $l^2(\mathbb{Z}^2)$, the family $\{g_k^{(l)}[\boldsymbol{n} - \boldsymbol{S}_k^{(l)}\boldsymbol{m}]\}_{0 \leq k \leq 2^l, \boldsymbol{m} \in \mathbb{Z}^2}$ ($\boldsymbol{m}$ is the location index) provides a basis for $y[\boldsymbol{n}]$, which is generated by translating the impulse responses of $G_k^{(l)}$ and demonstrates the directional and localized properties.

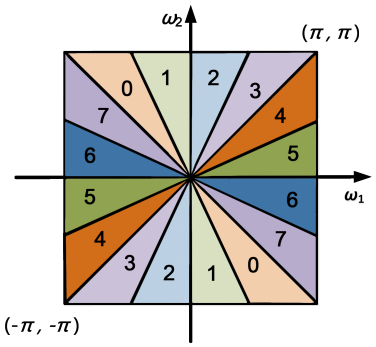

Fig. 5. Frequency partitioning with 8-direction wedge-shape subbands.

In order to obtain the corresponding coefficient images with contourlet transform, we use PDFB to decompose the image iteratively as shown in Fig. 6. The details are described as follows:

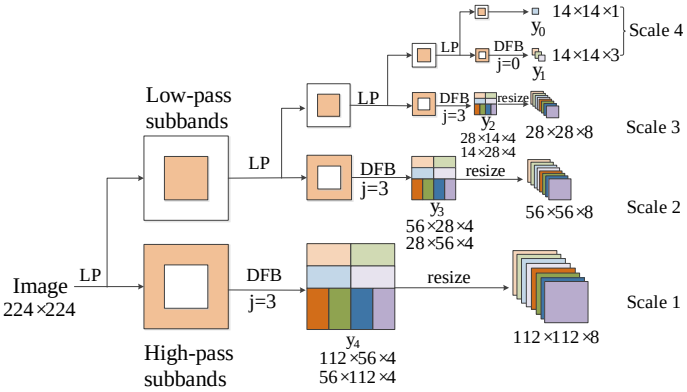

Fig. 6. The contourlet transform of an input image with size of 224×224. The decomposition level of LP is 4. The numbers of DFB are [0, 3, 3, 3] from coarse to fine scale, where 0 denoted a 2-D wavelet decomposition. The numbers below coefficient images denote $width \times height \times channels$ of the output.

Given an input image $\boldsymbol{x} \in \mathbb{R}^{n \times n}(n = 224)$, l = 1,...,L. L is the decomposition level of LP which represents scales, $k \in [0, 2^j]$ is the subbands index in each decomposition level j of DFB which represents directions. Using Eq.(10) to obtain a group of coefficients denoted $C_k^l(x, y)$. Therefore, different scales $\frac{n}{2^j} \times \frac{n}{2^j}$(112x112, 56x56, 28x28, 14x14) are obtained after LP decomposition with L = 4. The numbers of DFB are [0, 3, 3, 3] from coarse to fine scale, where 0 denoted a 2-D wavelet decomposition, resulting a coarse approximation y_0 and three bandpass directional subbands y_1 in scale 4. The 8 bandpass directional subbands are obtained from scale1 to scale3, respectively. When the decomposition level of DFB is even, the shape of band-pass subbands is square, and it is rectangular when the decomposition level is odd. Thus the decomposed images need to be processed before

concatenation. More details of multi-feature fusion can refer to Section II-*B*-3. The processed coefficient maps from scale1 to scale4 correspond to the spectral feature maps of orange in conv1, conv2, conv4 and conv6 in Fig. 2, respectively.

In C-CNN, we utilize 3x3 convolution operation with 1x1 padding and stride of 2 rather than pooling operation. It is vital to realize that the role of convolution layers in CNN is very similar to filter banks in traditional texture analysis. However, the spatial features extracted from CNN could be less dominant in texture analysis [49]. Therefore, we want to get more spectral information of texture.

*3) **Multi-feature fusion**:* In order to make full use of spectral features, spatial-spectral feature fusion via contourlet is applied to obtain more abundant spectral information. In addition, statistical features are flattened and concatenated to the FC layer, for the purpose of increasing the distinction between classes. More details are as follows.

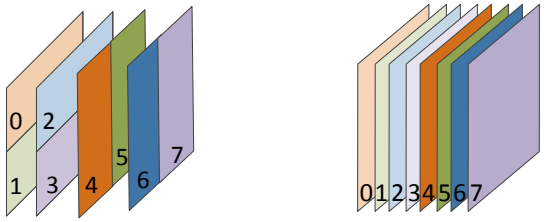

(a) (b)

Fig. 7. The process of 8 coefficients images before fusion. (a) Splicing the elongated coefficients images into squares. (b) Resizing the elongated decomposed images into squares.

Spatial-spectral feature fusion via contourlet: During the feature fusion, it needs to be considered how to concatenate the feature maps obtained by CNN and the contourlet decomposition images in corresponding sizes, since contourlet has elongated supports. For example, when the number of directional filter bank decomposition level is 3, resulting 2^3=8 wedge-shaped subbands in the frequency domain as shown in Fig. 5. The image is then decomposed into 8 subbands with rectangle-shaped [see Fig. 6]. In order to concatenate contourlet decomposition images to the network, the decomposed image should be treated as square before concatenation. Fig. 7 shows the two strategies to process the decomposed images. Contrast experiments are carried out by two strategies: splicing the feature maps of several elongated images into squares [see Fig. 7(a)], and resizing the elongated decomposed images directly to its corresponding sizes [see Fig. 7(b)]. We adopted the latter, which is in line with our intuition: the spatial and spectral features in texture images, the two different but related features can alternatively assist each other to obtain better local optima. For texture image decomposition with contourlet, where the coefficients are large is where the edges and textures are sensitive, and each pixel corresponds to a spatial coordinate. Therefore, the resized high-frequency coefficient maps can be consistent with spatial feature maps in pixel-wise fashion. The experiment [see Section III-*A*-3] shows the effectiveness of the spatial-spectral feature fusion via contourlet though its easy to implement.

Statistical feature fusion: Given an image *I*, we can obtain different coefficients $C_n(I)$ of various scales and directions with the contourlet decomposition. The subscript *n* is the index of coefficients. The mean μ_n and variance σ_n are chosen as the texture features of decomposed images, thus the statistical texture feature f is formulated as follows:

$$\begin{aligned} f &= (\mu_1, \sigma_1, \mu_2, \sigma_2, \ldots, \mu_{2^l}, \sigma_{2^l}) \\ \mu_n &= \frac{1}{W \times H} \sum_{x=1}^{W} \sum_{y=1}^{H} |C_n(x,y)| \\ \sigma_n &= \sqrt{\frac{1}{W \times H} \sum_{x=1}^{W} \sum_{y=1}^{H} (|C_n(x,y)| - \mu_n)^2} \end{aligned} \tag{12}$$

Where *l*=1, 2, . . . , *L*, represents the number of decomposition level. $C_n(x,y)$ is the *n*-th contourlet subband coefficients of an image. The width and height of the *n*-th subband is *W*, *H* separately.

Then the statistical texture feature f is concatenated to the features in FC2 layer, thus the concatenated features a_k can be expressed as:

$$a_k = f \bigoplus FC2, \tag{13}$$

where the symbol $\bigoplus$ denotes features concatenation.

*4) **Loss function and update rule**:* The softmax loss is applied to compute the multinomial logistic loss of the softmax using a single sample:

$$L = -log \frac{e^{a_j}}{\sum_{k=1}^{T} e^{a_k}}, \tag{14}$$

where a_k is the input and T denotes the number of classes. And we achieve stochastic optimization with Adam (adaptive moment estimation) [72], which is generated by combining the algorithm of Momentum [73] with RMSProp [74]. The update rule of Adam is:

$$\theta_{t+1} = \theta_t - \eta \frac{\hat{m}_t}{\sqrt{\hat{v}_t + \epsilon}}, \tag{15}$$

where θ_t is the parameter at timestep t and η is the learning rate. $\hat{m}_t = \frac{m_t}{1-\beta_1^t}$ and $\hat{v}_t = \frac{v_t}{1-\beta_2^t}$ are bias-corrected estimates of first (m_t) and second raw moment (v_t) of the gradients, respectively. The hyperparameters β_1, β_2 denote the exponential decay rates with the constraint: $0 \leq \beta_1, \beta_2 < 1$.

C. Implementation of C-CNN

The proposed Contourlet CNN (C-CNN) architecture is derived from AlexNet as can be found from Fig. 2. It consists of 9 convolution layers, 1 global average pooling layer followed by 3 fully-connected layers. 3×3 kernels and 1×1 padding are applied in convolution layers, which guarantee the size of the feature maps. We utilize stride of 2 in convolution layers instead of pooling. The learning procedure is listed in **Algorithm 1**. *k* is the subbands index in F_{DFB} and the decomposition level *L*=4. Softmax Loss and Adam algorithm are employed. The default values in Adam are $\beta_1 = 0.9$, $\beta_2 = 0.999$, $\epsilon = 10^{-8}$. As explained in [75] that average pooling improved the gradient flow in texture generation rather

than max pooling, thus the global average pooling (GAP) layer was employed in our network. The invariance size of feature maps is ensured by the 2-pixel stride in the convolutional layer with 1x1 padding. The size of the output layer is equal to the number of classes. Some regular operations are adopted in our network such as batch normalization and dropout. We implement our network on Caffe and the memory consumption of our model is 52.9 MB.

Algorithm 1 Learning Procedure of C-CNN

Input: Training dataset: $\boldsymbol{x} = \{x_n | n = 1, 2, \ldots, N\}$, and their corresponding labels $\boldsymbol{y} = \{y_n | n = 1, 2, \ldots, N\}$; the number of categories *T*.

Output: Classification result $\hat{\boldsymbol{y}} = \{\hat{y}_n | n = 1, 2, \ldots, N\}$.

Preparation: The backbone network can be simply expressed as [*conv1*, …, *conv9*, *GAP*, *FC1*, *FC2*, *FC3*], *nlevels* = [0, 3, 3, 3] , $l = 1, \ldots, L$, F_{LP} = 'maxflat', F_{DFB} ='dmaxflat7'.
Begin
for *n* = 1 to *N* **do**
  Given an input image x_n, using Eq.(10) to obtain a group of coefficients denoted $C_k^l(x, y)$. k is the subbands index in each decomposition level;
  Calculate the statistical feature f of $C_k^l(x, y)$ by Eq.(12);
  if $height(C_k^l(x, y)) \neq width(C_k^l(x, y))$ **then**
    resize the $C_k^l(x, y)$ to the size of M^2, where $M = max(height(C_k^l(x, y)), width(C_k^l(x, y)))$.
  end if
  Cascade the feature maps as $conv1 \bigoplus C_k^l(x, y)$, $conv2 \bigoplus C_k^2(x, y)$,$conv4 \bigoplus C_k^3(x, y)$,$conv6 \bigoplus C_k^4(x, y)$;
  Concatenate statistical feature to *FC2*: $f \bigoplus FC2$;
  Minimize Eq.(14) and update the parameters by Eq.(15) until convergence.
end for
End

We concatenated the feature maps obtained by CNN and the contourlet decomposition images in corresponding sizes. The contourlet decomposition is achieved by using filters "maxflat" for the pyramidal decomposition and "dmaxflat7" for the directional decomposition. The numbers of directional filter bank decomposition levels at each pyramidal level is [0, 3, 3, 3] from coarse to fine scale, where 0 denoted a 2-D wavelet decomposition. The interlaced down sampling factor *p*=2.

In order to make full use of the spectral information in the decomposed images, we use the spatial-spectral feature fusion and statistical feature fusion. Spatial-spectral feature fusion strengthens the correlation between feature maps in different domains. Statistical features are commonly used in traditional texture classification, which is a good representation of texture in a coarse degree. Thus we calculate the mean and variance of each contourlet subband coefficient. Then, these features (dimension is 56) are connected to the FC layer. It enhanced feature representation, rotation invariant, and intra-class disparity to some extent.

III. Validation and generalization

In this section, the proposed C-CNN is evaluated on 8 benchmark datasets: 3 texture datasets for image texture classification (Section III-A) and 5 remote sensing datasets for remote sensing scene classification (Section III-B). We also check the influence of parameters in C-CNN, and evaluate the effectiveness of the proposed network components.

A. Image texture classification

We evaluated C-CNN on three benchmark datasets: kth-tips2-b [76], DTD [77] and CUReT [78]. The kth-tips2-b dataset is composed of 11 classes of texture images with 1 training sample and 3 testing samples. Each sample contains 4x3x9=108 texture images under 4 illumination conditions, 3 poses and 9 scales with the size of 200x200. The results are averaged in the 4 train-val-test splits on the kth-tips2-b evaluation. The Describable Texture Datasets (DTD) is composed of 47 classes of 120 images, providing 10 splits into equal size of 40 training images, 40 validation images and 40 test images. For this dataset, we apply the same evaluation as is used in the kth-tips2-b dataset, which averages the results on the 10 train-val-test splits.

The Columbia-Utrecht Reflection and Texture (CUReT) dataset collects 61 classes of real-world surfaces which covers a wide range of geometric and photometric properties. 205 samples per class with the size of 640x480. We use 92 images for each class: 46 for training and the rest for testing, and cropped the region (200x200) as in [37]. The results are averaged over the random 10 splits. All the images of the datasets are resized into 224x224.

1) Networks from scratch and pre-trained: We applied C-CNN to these two widely used texture datasets: kth-tips2-b and DTD. The classification results are reported in TABLE I. The strategy of "pre-trained" is the method on ImageNet. TABLE I demonstrates the accuracy of C-CNN reaches 70.31% and 40.62% on the kth-tips2-b dataset and the DTD dataset, respectively. The proposed method is compared with AlexNet [56], the spectral method with shearlet transform [20], T-CNN [47] and Wavelet CNN [49]. The comparison results indicate that the proposed method describing textures at multiple scales and directions has great potential for texture classification.

TABLE I
Classification results (accuracy %) for networks.

Methods	Strategy	kth-tips2-b	DTD
AlexNet [56]	not pre-trained	$48.3 \pm_{1.4}$	$22.7 \pm_{1.3}$
T-CNN [47]	not pre-trained	$48.7 \pm_{1.3}$	$27.8 \pm_{1.2}$
	pre-trained	$73.2 \pm_{2.2}$	$55.8 \pm_{0.8}$
Shearlet [20]	pre-trained	$62.3 \pm_{0.8}$	$21.6 \pm_{0.9}$
Wavelet CNN [49]	not pre-trained	$63.7 \pm_{2.3}$	$35.6 \pm_{0.7}$
	pre-trained	$74.2 \pm_{1.2}$	$59.8 \pm_{0.9}$
Contourlet CNN	not pre-trained	$\mathbf{70.31} \pm_{1.6}$	$\mathbf{40.62} \pm_{1.7}$
	pre-trained	$\mathbf{79.25} \pm_{1.7}$	$\mathbf{61.03} \pm_{1.0}$

The proposed method is evaluated on the CUReT dataset. TABLE II reports the average classification accuracy of different methods. It can be found that C-CNN has comparable

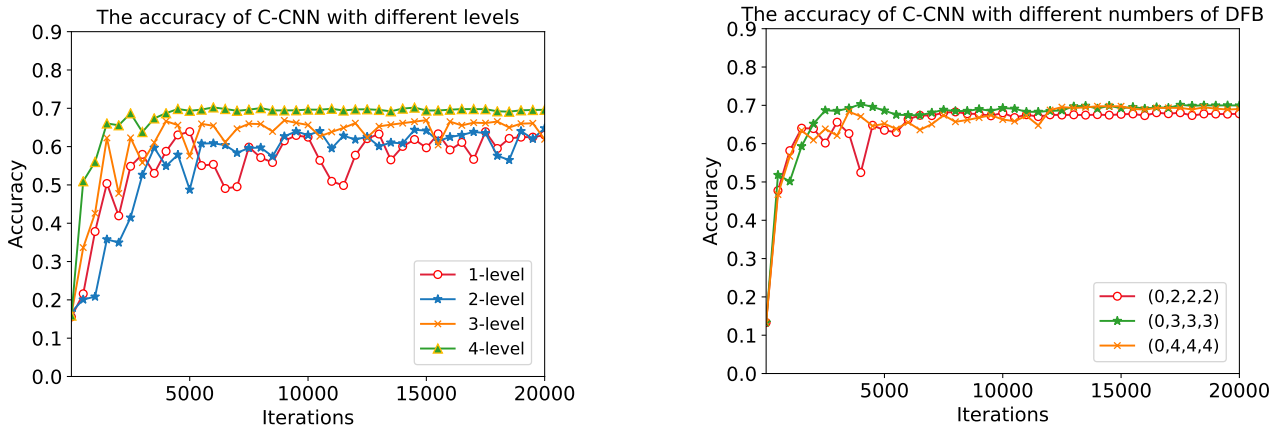

(a) (b)

Fig. 8. C-CNN parameters analysis. (a) The accuracy of C-CNN with different contourlet decomposition levels. (b) The accuracy of C-CNN with different numbers of directional filter bank.

accuracy (99.7%) with the state of the art (99.8%) [77]. Overall, the remarkable behaviors achieved on three public texture datasets indicate the superior discriminative capability of C-CNN. Furthermore, the C-CNN combines spectral features and spatial features at multi-scales with relatively sparse representation, which increased the interpretability of the network.

TABLE II
RESULTS (ACCURACY %) ON CURET DATASET.

Methods	Accuracy	Methods	Accuracy
LDTP [79]	91.54	AlexNet[56]	99.4
RALBGC [80]	93.82	T-CNN-1[47]	99.0
LCCMSP [81]	94.45	T-CNN-3[47]	99.5
ARCS-LBP [82]	94.72	IFV+ DeCAF[77]	**99.8**
LDEP [83]	95.23	IFV[77]	99.5
Wavelet CNN[49]	99.4	Contourlet CNN	99.7

2) Network parameter analysis: In the texture images, contourlet decomposition captures the spectral information at different scales and directions. Accordingly, we investigated the behavior of our Contourlet CNN on the kth-tips2-b dataset with various decomposition levels and various numbers of the DFB in TABLE III.

TABLE III
THE COMPARISON OF THE CLASSIFICATION RESULTS (ACCURACY %) WITH CONTOURLET CNN.

Methods	Accuracy	Methods	Accuracy
1-level C-CNN	$63.91\pm_{2.4}$	different numbers of DFB	
2-level C-CNN	$64.78\pm_{1.3}$	(0,2,2,2)	$68.28\pm_{1.2}$
3-level C-CNN	$66.90\pm_{2.1}$	(0,3,3,3)	$\mathbf{70.31}\pm_{1.6}$
4-level C-CNN	$\mathbf{70.31}\pm_{1.6}$	(0,4,4,4)	$69.77\pm_{1.1}$

In Fig. 8(a), we can see that the accuracies improved with an increase in the decomposition levels and the fluctuation gradually stabilized down. The results trained from scratch show that the proposed approach performs best with 4-level Contourlet CNN. It is consistent with our intuition: the more decomposition features extracted, the more representative information is generated. In terms of the optimal numbers of directional filter banks, [0, 3, 3, 3] is superior to the others as shown in Fig. 8(b).

3) Ablation study: In order to evaluate the effectiveness of the components in the proposed network, we experiment with several variants of the network [see TABLE IV] on the kth-tips2-b dataset. The "origin" splices the elongated decomposed images into its corresponding sizes, since contourlet has elongated supports. Spatial-Spectral Feature Fusion via contourlet (SSFF) represents the elongated decomposed images are directly resized into its corresponding sizes. Statistical Feature Fusion (SSF) denotes the additional texture features of decomposed images. More details of statistical features can refer to Section II-*B*-3.

TABLE IV
CLASSIFICATION RESULTS (ACCURACY %) OF SEVERAL VARIANTS WITH CONTOURLET CNN TRAINED FROM SCRATCH.

origin	SSFF	SSF	accuracy
√			$64.70\pm_{2.3}$
√	√		$67.06\pm_{1.9}$
√	√	√	$70.31\pm_{1.6}$

The "origin" version of contourlet CNN achieved an accuracy of 0.84 on additional datasets of kth-tips2-b which contains 4 classes of 36 images with no pre-trained. In addition, we evaluated the performance of contourlet CNN in remote sensing scene classification.

B. Remote sensing scene classification

We also evaluated C-CNN on another five benchmark datasets of remote sensing: UC Merced dataset (UCM) [84], WHU-RS dataset [85], AID dataset [86], RSSCN7 dataset [87] and NWPU-RESISC45 [88]. The UCM dataset is collected from the USGS National Map Urban Area Imagery in various urban areas with the pixel resolution of 1 foot. It composed of 21 classes of 100 images with the size of 256x256 pixels. 80 training images per category are randomly selected and

the remaining 20 images for the testing set. The results are averaged on the 10 train-val-test splits in random on the UCM evaluation.

The satellite images in the WHU-RS dataset are exported from Google Earth with high-resolution up to 0.5 m. It composed of 19 classes of 50 images with the size of 600x600 pixels. For this dataset, we apply the same evaluation as was used in the UCM dataset, which averages the results on the 10 train-val-test splits. 30 training images per category are randomly selected and the remaining 20 images for the testing set.

The AID dataset is collected from Google Earth imagery which contains 10000 images within 30 classes. It is in a multisource condition with the size of 600x600. Unlike the single source images datasets, the AID is challenging since images are extracted at different times and seasons with various resolutions. The RSSCN7 dataset is also collected from Google Earth which includes 7 categories of 400 images with the size of 400x400 pixels. Images are sampled at 4 different scales with 100 images per scale in each class under varying seasons and weathers. 50% samples are fixed for training both in the RSSCN7 and AID datasets. We average the results on the 10 train-val-test splits and resize all the images of the datasets to 224x224.

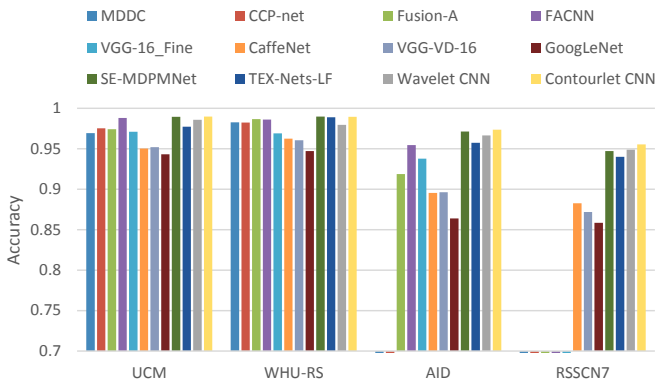

Fig. 9. Results of the accuracy on the four datasets.

The NWPU-RESISC45 dataset is created by Northwestern Polytechnical University (NWPU) from Google Earth, which is used for remote sensing image scene classification (RESISC). This dataset includes 31,500 images, covering 45 scene classes of 700 images with the size of 256x256. The spatial resolution of these images varies from about 30 to 0.2 m per pixel for most scene classes. The dataset is challenging since images are captured at different weather conditions and imaging angles from different sensors. The training ratios are 10% and 20%, respectively. The overall accuracy is averaged on the 10 train-val-test splits.

The visual classification results on the four remote sensing scene datasets are shown in Fig. 9, and the quantitative results are listed in TABLE V.

The comparison methods are considered as follows:

- *MDDC* [89]: The multiscale deeply described correlatons method incorporates appearance and spatial features at different scales to obtain an accurate classification of the land-use scene images.
- *CCP-net* [90]: It proposes an end-to-end trainable CNNs which generates a spatial-rotation-invariant representation with concentric circle pooling.
- *Fusion-A* [91]: It builds the fusion by addition strategy on high-level features extracted from CaffeNet, VGG-VD-16, and GoogLeNet in [86].
- *FACNN* [92]: It achieves the remote sensing scene classification in the feature aggregation CNN, which describes the intermediate features with convolutional features encoding module and the progressive aggregation strategy.
- *VGG-16_Fine* [92] It employs the VGG-16 trained on ImageNet to initialize the weight parameteris of the network.
- *CaffeNet* [86]: It comprises five convolutional layers, each followed by a pooling layer and three fully connected layers.
- *VGG-VD-16* [86]: It composed of 13 convolutional layers and 3 fully connected layers.
- *GoogLeNet* [86]: It is a 22-layers architecture with the inception modules.
- *SE-MDPMNet* [93]: It extracts effective multi-scale features with the dilated convolution, multidilation pooling module and channel attention in MobileNet V2 which maintains high accuracy.
- *TEX-Nets-LF* [94]: It uses the late fusion strategy on two-stream deep architectures, combining the texture and color information as complementary.
- *Wavelet CNN* [49]: It integrates a spectral analysis of wavelet into CNNs, based on the insight that the pooling and the convolution can be thought as a limited form of spectral analysis.

TABLE V
CLASSIFICATION RESULTS (ACCURACY %) FOR NETWORKS.

Methods	UCM	WHU-RS	AID	RSSCN7
MDDC [89]	$96.92\pm_{0.57}$	$98.27\pm_{0.53}$	-	-
CCP-net [90]	$97.52\pm_{0.97}$	$98.23\pm_{0.40}$	-	-
Fusion-A [91]	$97.42\pm_{1.79}$	$98.65\pm_{0.43}$	$91.87\pm_{0.36}$	-
FACNN [92]	$98.81\pm_{0.24}$	$98.61\pm_{0.44}$	$95.45\pm_{0.11}$	-
VGG-16_Fine [92]	$97.10\pm_{0.51}$	$96.91\pm_{0.21}$	$93.78\pm_{0.36}$	-
CaffeNet [86]	$95.02\pm_{0.81}$	$96.24\pm_{0.56}$	$89.53\pm_{0.31}$	$88.25\pm_{0.62}$
VGG-VD-16 [86]	$95.21\pm_{1.20}$	$96.05\pm_{0.91}$	$89.64\pm_{0.36}$	$87.18\pm_{0.94}$
GoogLeNet [86]	$94.31\pm_{0.89}$	$94.71\pm_{1.33}$	$86.39\pm_{0.55}$	$85.84\pm_{0.92}$
SE-MDPMNet [93]	$98.95\pm_{0.12}$	$\mathbf{98.97}\pm_{0.24}$	$97.14\pm_{0.15}$	$94.71\pm_{0.15}$
TEX-Nets-LF [94]	$97.72\pm_{0.54}$	$98.88\pm_{0.49}$	$95.73\pm_{0.16}$	$94.0\pm_{0.57}$
Wavelet CNN [49]	$98.58\pm_{0.13}$	$97.96\pm_{0.90}$	$96.65\pm_{0.24}$	$94.89\pm_{0.67}$
Contourlet CNN	$\mathbf{98.97}\pm_{0.21}$	$98.95\pm_{0.82}$	$\mathbf{97.36}\pm_{0.45}$	$\mathbf{95.54}\pm_{0.71}$

It shows that C-CNN achieves comparable performance on three datasets compared with other studied approaches, while it is inferior to the SE-MDPMNet [93] of 0.02% on the WHU-RS dataset. The reasons for the competitive performance are as follows: First, the multi-scale and multi-directional features of contourlet can be associated with a biological interpretation of HVS. Second, the remote sensing images are mainly composed of geometrical and morphological features, which are con-

sistent with the characteristics of multi-scale geometry. Thus we have embedded a priori knowledge into CNNs to refine the network. Third, wavelet CNN [49] employs the constant parameters of filters, which is better than the one with single CNNs. The contourlet has more sparse feature representation than wavelet, and the additional statistical features enhanced feature representation, as well as increased intra-class disparity to some extent. So the effective performances are obtained with the singularity and directionality of the contours.

TABLE VI
CLASSIFICATION RESULTS (ACCURACY %) ON NWPU-RESISC45 DATASET.

Methods	Training ratios	
	10%	20%
unsupervised feature learning methods		
BoVW+SPM [88]	$27.83\pm_{0.61}$	$32.96\pm_{0.47}$
LLC [88]	$38.81\pm_{0.23}$	$40.03\pm_{0.34}$
BoVW [88]	$41.72\pm_{0.21}$	$44.97\pm_{0.28}$
CNN-based methods		
AlexNet [88]	$76.69\pm_{0.21}$	$79.85\pm_{0.13}$
VGGNet-16 [88]	$76.47\pm_{0.18}$	$79.79\pm_{0.15}$
GoogLeNet [88]	$76.19\pm_{0.38}$	$78.48\pm_{0.26}$
LASC-CNN [95]	81.37	84.30
BoCF(VGGNet-16) [96]	$82.65\pm_{0.31}$	$84.32\pm_{0.17}$
Attention GANs [97]	$\mathbf{86.11}\pm_{0.22}$	$89.44\pm_{0.18}$
Two-stream fusion [98]	$85.02\pm_{0.25}$	$87.01\pm_{0.19}$
Wavelet CNN [49]	$84.69\pm_{0.44}$	$88.84\pm_{0.38}$
Contourlet CNN	$85.93\pm_{0.51}$	$\mathbf{89.57}\pm_{0.45}$

TABLE VI reports the comparative results on the NWPU-RESISC45 dataset, which includes the representative approaches. Namely, unsupervised feature learning methods and CNN-based methods. Among them, BoVW+SPM [88], LLC [88] and BoVW [88] are unsupervised feature learning methods. AlexNet [88], VGGNet-16 [88], GoogLeNet [88], LASC-CNN [95], BoCF(VGGNet-16) [96], Attention GANs [97], Two-stream fusion [98], Wavelet CNN [49] and the proposed method are CNN-based methods. As can be seen in TABLE VI, the CNN-based methods perform much better than unsupervised feature learning methods under the training ratios of 10% and 20%. In addition, the proposed method surpasses most of the CNN-based methods which deal with the scene classification task in the spatial domain. The proposed method achieves an accuracy of 85.93 ± 0.51 (10% training samples) and 89.57 ± 0.45 (20% training samples). The improvements may come from the combination of the spatial and spectral features. This is due to the fact that the information of two domains have supplied complementary components, and the statistical features can enhance the discrimination of global scene representation. Besides, compared to other CNN-based methods, the proposed model is more compact which has the advantage of relative shadow structure in small network size.

IV. CONCLUDING REMARKS

In this paper, Contourlet CNN is presented to extract and integrate spatial and spectral features for texture classification. Contourlet transform provides more multidirectional and multiscale information effectively in the spectral domain. It is novel that the spectral analysis is integrated into CNN with statistical properties for texture sparse representation. The correlation between feature maps in different domains is strengthened by the spatial-spectral feature fusion via contourlet at different decomposition levels. And the additional statistical features enhanced the discriminative feature representation and rotation invariant.

The theoretical analysis and complete experiments on C-CNN are discussed in this paper. The proposed method can achieve comparable results against the state-of-the-art methods on three texture datasets and five remote sensing datasets with effectiveness and reliability. In terms of the model generality, a good feature representation can be obtained without pre-training, thus the model can be employed in other related visual tasks. However, there are still limitations on the adaptive selection of the contourlet decomposition basis on different tasks. And the contourlet kernel is integrated to the network explicitly. In future studies, we plan to incorporate a guide attention strategy into our model to make full use of spectral information.

REFERENCES

[1] R. M. Haralick, K. Shanmugam, and I. Dinstein, "Textural features for image classification," *IEEE Transactions on Systems, Man, and Cybernetics*, vol. SMC-3, no. 6, pp. 610–621, Nov. 1973.

[2] L. Liu and P. Fieguth, "Texture classification from random features," *IEEE Transactions on Pattern Analysis and Machine Intelligence*, vol. 34, no. 3, pp. 574–586, Mar. 2012.

[3] B. Julesz, "Visual pattern discrimination," *IRE Transactions on Information Theory*, vol. 8, no. 2, pp. 84–92, Feb. 1962.

[4] C.-M. Wu and Y.-C. Chen, "Statistical feature matrix for texture analysis," *CVGIP: Graphical Models and Image Processing*, vol. 54, no. 5, pp. 407 – 419, 1992.

[5] J. S. Weszka, C. R. Dyer, and A. Rosenfeld, "A comparative study of texture measures for terrain classification," *IEEE Transactions on Systems, Man, and Cybernetics*, vol. SMC-6, no. 4, pp. 269–285, Apr. 1976.

[6] D. Blostein and N. Ahuja, "Shape from texture: integrating texture-element extraction and surface estimation," *IEEE Transactions on Pattern Analysis and Machine Intelligence*, vol. 11, no. 12, pp. 1233–1251, Dec. 1989.

[7] K. A. Stevens, "Surface perception from local analysis of texture," in *AI-Tech. Rep.-512*. AI Laboratory, Massachusetts Institute of Technology Cambridge, 1980.

[8] T. Ojala, M. Pietikainen, and D. Harwood, "Performance evaluation of texture measures with classification based on kullback discrimination of distributions," vol. 1, pp. 582–585, Oct. 1994.

[9] L. Wang and D.-C. He, "Texture classification using texture spectrum," *Pattern Recognition*, vol. 23, no. 8, pp. 905–910, 1990.

[10] T. Ojala, M. Pietikäinen, and D. Harwood, "A comparative study of texture measures with classification based

on featured distributions," *Pattern Recognition*, vol. 29, no. 1, pp. 51–59, 1996.

[11] T. Ojala, M. Pietikainen, and T. Maenpaa, "Multiresolution gray-scale and rotation invariant texture classification with local binary patterns," *IEEE Transactions on Pattern Analysis and Machine Intelligence*, vol. 24, no. 7, pp. 971–987, 2002.

[12] Y. Zhao, W. Jia, R.-X. Hu, and H. Min, "Completed robust local binary pattern for texture classification," *Neurocomputing*, vol. 106, pp. 68–76, 2013.

[13] R. Chellappa and S. Chatterjee, "Classification of textures using gaussian markov random fields," *IEEE Transactions on Acoustics, Speech, and Signal Processing*, vol. 33, no. 4, pp. 959–963, 1985.

[14] A. Khotanzad and R. L. Kashyap, "Feature selection for texture recognition based on image synthesis," *IEEE Transactions on Systems, Man, and Cybernetics*, vol. 17, no. 6, pp. 1087–1095, 1987.

[15] B. J. Super and A. C. Bovik, "Localized measurement of image fractal dimension using gabor filters," *Journal of visual communication and image representation*, vol. 2, no. 2, pp. 114–128, 1991.

[16] J. M. Coggins and A. K. Jain, "A spatial filtering approach to texture analysis," *Pattern Recognition Letters*, vol. 3, no. 3, pp. 195–203, 1985.

[17] L. M. Kaplan, "Extended fractal analysis for texture classification and segmentation," *IEEE Transactions on Image Processing*, vol. 8, no. 11, pp. 1572–1585, 1999.

[18] H. Arof and F. Deravi, "Circular neighbourhood and 1-D DFT features for texture classification and segmentation," *IEE Proceedings-Vision, Image and Signal Processing*, vol. 145, no. 3, pp. 167–172, 1998.

[19] Q. Sun, B. Hou, and L.-c. Jiao, "Automatic texture segmentation based on wavelet-domain hidden markov tree," in *Iberoamerican Congress on Pattern Recognition*. Springer, 2005, pp. 470–480.

[20] K. G. Krishnan, P. Vanathi, and R. Abinaya, "Performance analysis of texture classification techniques using shearlet transform," in *2016 International Conference on Wireless Communications, Signal Processing and Networking (WiSPNET)*. IEEE, 2016, pp. 1408–1412.

[21] Y. Dong, D. Tao, X. Li, J. Ma, and J. Pu, "Texture classification and retrieval using shearlets and linear regression," *IEEE Transactions on Cybernetics*, vol. 45, no. 3, pp. 358–369, 2014.

[22] C. Vivek and S. Audithan, "Classification of colour textures using shearlets," in *International Conference on Information Communication and Embedded Systems (ICICES2014)*. IEEE, 2014, pp. 1–5.

[23] K. Huang and S. Aviyente, "Rotation invariant texture classification with ridgelet transform and fourier transform," in *2006 International Conference on Image Processing*. IEEE, 2006, pp. 2141–2144.

[24] Y. Shang, Y.-H. Diao, and C.-M. Li, "Rotation invariant texture classification algorithm based on curvelet transform and SVM," in *2008 International Conference on Machine Learning and Cybernetics*, vol. 5. IEEE, 2008, pp. 3032–3036.

[25] Z. Xiangbin, "Texture classification based on contourlet and support vector machines," in *2009 ISECS International Colloquium on Computing, Communication, Control, and Management*, vol. 2. IEEE, 2009, pp. 521–524.

[26] Y. Hu, B. Hou, S. Wang, and L. Jiao, "Texture classification via stationary-wavelet based contourlet transform," in *International Workshop on Intelligent Computing in Pattern Analysis and Synthesis*. Springer, 2006, pp. 485–494.

[27] Y. Sha, L. Cong, Q. Sun, and L. Jiao, "Unsupervised image segmentation using contourlet domain hidden markov trees model," in *International Conference Image Analysis and Recognition*. Springer, 2005, pp. 32–39.

[28] Xiao-Qing Shang, Guo-Xiang Song, and Biao Hou, "Content based texture image classification," in *Proceedings of the 2003 International Conference on Machine Learning and Cybernetics*, vol. 3, Nov. 2003, pp. 1309–1313.

[29] T. Shan, X. Zhang, and L. Jiao, "A brushlet-based feature set applied to texture classification," in *International Conference on Computational and Information Science*. Springer, 2004, pp. 1175–1180.

[30] C. Lin, S. Yuheng, H. Biao, and J. Licheng, "Unsupervised image segmentation based on the anisotropic texture information," in *Third International Conference on Image and Graphics (ICIG'04)*. IEEE, 2004, pp. 124–127.

[31] L. Chen and H. Man, "Hybrid IMM/SVM approach for wavelet-domain probabilistic model based texture classification," *IEE Proceedings-Vision, Image and Signal Processing*, vol. 152, no. 6, pp. 724–730, 2005.

[32] K. I. Kim, K. Jung, S. H. Park, and H. J. Kim, "Support vector machines for texture classification," *IEEE Transactions on Pattern Analysis and Machine Intelligence*, vol. 24, no. 11, pp. 1542–1550, 2002.

[33] S. Liu, H. Yi, L.-T. Chia, and D. Rajan, "Adaptive hierarchical multi-class svm classifier for texture-based image classification," in *2005 IEEE International Conference on Multimedia and Expo*. IEEE, 2005.

[34] I. Turkoglu and E. Avci, "Comparison of wavelet-svm and wavelet-adaptive network based fuzzy inference system for texture classification," *Digital Signal Processing*, vol. 18, no. 1, pp. 15–24, 2008.

[35] E. P. Lam, "Texture classification using wavelet decomposition," in *2008 IEEE International Conference on System of Systems Engineering*. IEEE, 2008, pp. 1–5.

[36] Z. Sun and K. Jia, "Road surface condition classification based on color and texture information," in *2013 Ninth International Conference on Intelligent Information Hiding and Multimedia Signal Processing*. IEEE, Oct. 2013, pp. 137–140.

[37] Z. Guo, L. Zhang, and D. Zhang, "A completed modeling of local binary pattern operator for texture classification," *IEEE Transactions on Image Processing*, vol. 19, no. 6, pp. 1657–1663, 2010.

[38] G. Girish and J. K. Dash, "Adaptive fuzzy local binary pattern for texture classification," in *2017 2nd International Conference on Man and Machine Interfacing*

(MAMI). IEEE, 2017, pp. 1–5.

[39] G. S. Raghtate and S. S. Salankar, "Comparison of classification methods with second order statistical analysis and wavelet transform for texture image classification," in *2015 International Conference on Computational Intelligence and Communication Networks (CICN)*, Dec. 2015, pp. 312–317.

[40] R. Paget, I. Longstaff, and B. Lovell, "Texture classification using nonparametric markov random fields," in *Proceedings of 13th International Conference on Digital Signal Processing*, vol. 1. IEEE, 1997, pp. 67–70.

[41] X. Bai and K. Wang, "Research on classification of wood surface texture based on markov random field," in *2007 2nd IEEE Conference on Industrial Electronics and Applications*. IEEE, 2007, pp. 664–668.

[42] H. Potlapalli and R. C. Luo, "Fractal-based classification of natural textures," *IEEE Transactions on Industrial Electronics*, vol. 45, no. 1, pp. 142–150, 1998.

[43] L. Jiao, L. Bo, and L. Wang, "Fast sparse approximation for least squares support vector machine," *IEEE Transactions on Neural Networks*, vol. 18, no. 3, pp. 685–697, 2007.

[44] Q. Li, W. Cai, X. Wang, Y. Zhou, D. D. Feng, and M. Chen, "Medical image classification with convolutional neural network," in *2014 13th International Conference on Control Automation Robotics & Vision (ICARCV)*. IEEE, 2014, pp. 844–848.

[45] L. G. Hafemann, L. S. Oliveira, and P. Cavalin, "Forest species recognition using deep convolutional neural networks," in *2014 22nd International Conference on Pattern Recognition*. IEEE, 2014, pp. 1103–1107.

[46] M. Cimpoi, S. Maji, and A. Vedaldi, "Deep filter banks for texture recognition and segmentation," in *Proceedings of the IEEE Conference on Computer Vision and Pattern Recognition*, 2015, pp. 3828–3836.

[47] V. Andrearczyk and P. F. Whelan, "Using filter banks in convolutional neural networks for texture classification," *Pattern Recognition Letters*, vol. 84, pp. 63–69, 2016.

[48] S. Fujieda, K. Takayama, and T. Hachisuka, "Wavelet convolutional neural networks for texture classification," *arXiv preprint arXiv:1707.07394*, 2017.

[49] S. Fujieda, K. Takayama, and T. Hachisuka, "Wavelet convolutional neural networks," *arXiv preprint arXiv:1805.08620*, 2018.

[50] K. He, X. Zhang, S. Ren, and J. Sun, "Deep residual learning for image recognition," in *Proceedings of the IEEE Conference on Computer Vision and Pattern Recognition*, 2016, pp. 770–778.

[51] G. Huang, Z. Liu, L. Van Der Maaten, and K. Q. Weinberger, "Densely connected convolutional networks," in *Proceedings of the IEEE Conference on Computer Vision and Pattern Recognition*, 2017, pp. 4700–4708.

[52] M. Lin, Q. Chen, and S. Yan, "Network In Network," in *International Conference on Learning Representations*, 2014.

[53] S. Mallat, *A Wavelet Tour of Signal Processing, 2nd Edition*. Elsevier, 1999.

[54] M. Do and M. Vetterli, "Contourlets, beyond wavelets," *New York, NY, USA: Academic*, 2003.

[55] D. H. Hubel and T. N. Wiesel, "Receptive fields and functional architecture in two nonstriate visual areas (18 and 19) of the cat," *Journal of neurophysiology*, vol. 28, no. 2, pp. 229–289, 1965.

[56] I. Sutskever, G. E. Hinton, and A. Krizhevsky, "Imagenet classification with deep convolutional neural networks," *Advances in neural information processing systems*, pp. 1097–1105, 2012.

[57] K. Chatfield, K. Simonyan, A. Vedaldi, and A. Zisserman, "Return of the devil in the details: Delving deep into convolutional nets," in *British Machine Vision Conference 2014*, 2014.

[58] E. Shelhamer, J. Long, and T. Darrell, "Fully convolutional networks for semantic segmentation," *IEEE Transactions on Pattern Analysis and Machine Intelligence*, vol. 39, no. 4, pp. 640–651, Apr. 2017.

[59] F. Liu, L. Jiao, and X. Tang, "Task-oriented GAN for PolSAR image classification and clustering," *IEEE Transactions on Neural Networks and Learning Systems*, vol. 30, no. 9, pp. 2707–2719, Sept. 2019.

[60] R. Girshick, J. Donahue, T. Darrell, and J. Malik, "Rich feature hierarchies for accurate object detection and semantic segmentation," in *Proceedings of the IEEE Conference on Computer Vision and Pattern Recognition*, 2014, pp. 580–587.

[61] F. H. C. Tivive and A. Bouzerdoum, "Texture classification using convolutional neural networks," in *TENCON 2006-2006 IEEE Region 10 Conference*. IEEE, 2006, pp. 1–4.

[62] M. N. Do and M. Vetterli, "Contourlets: a directional multiresolution image representation," in *Proceedings. International Conference on Image Processing*, vol. 1, Sept. 2002, pp. I–357–I–360.

[63] B. A. Olshausen and D. J. Field, "Emergence of simple-cell receptive field properties by learning a sparse code for natural images," *Nature*, vol. 381, no. 6583, pp. 607–609, 1996.

[64] D. L. Donoho and A. G. Flesia, "Can recent innovations in harmonic analysisexplain'key findings in natural image statistics?" *Network: computation in neural systems*, vol. 12, no. 3, pp. 371–393, 2001.

[65] M. N. Do and M. Vetterli, "The contourlet transform: an efficient directional multiresolution image representation," *IEEE Transactions on Image Processing*, vol. 14, no. 12, pp. 2091–2106, 2005.

[66] D. L. Donoho, M. Vetterli, R. A. DeVore, and I. Daubechies, "Data compression and harmonic analysis," *IEEE Transactions on Information Theory*, vol. 44, no. 6, pp. 2435–2476, 1998.

[67] E. J. Candès and D. L. Donoho, "New tight frames of curvelets and optimal representations of objects with piecewise C2 singularities," *Communications on Pure and Applied Mathematics: A Journal Issued by the Courant Institute of Mathematical Sciences*, vol. 57, no. 2, pp. 219–266, 2004.

[68] L. Jiao, J. Pan, and Y. Fang, "Multiwavelet neural network and its approximation properties," *IEEE Transac-*

tions on neural networks, vol. 12, no. 5, pp. 1060–1066, 2001.

[69] P. Burt and E. Adelson, "The laplacian pyramid as a compact image code," *IEEE Transactions on Communications*, vol. 31, no. 4, pp. 532–540, 1983.

[70] R. H. Bamberger and M. J. Smith, "A filter bank for the directional decomposition of images: Theory and design," *IEEE Transactions on Signal Processing*, vol. 40, no. 4, pp. 882–893, 1992.

[71] M. N. Do and M. Vetterli, "Contourlets: a new directional multiresolution image representation," in *Conference Record of the Thirty-Sixth Asilomar Conference on Signals, Systems and Computers*, vol. 1, Nov. 2002, pp. 497–501.

[72] D. P. Kingma and J. Ba, "Adam: A method for stochastic optimization," in *3rd International Conference on Learning Representations*, 2015.

[73] N. Qian, "On the momentum term in gradient descent learning algorithms," *Neural networks*, vol. 12, no. 1, pp. 145–151, 1999.

[74] T. Tieleman and G. Hinton, "Lecture 6.5-rmsprop: Divide the gradient by a running average of its recent magnitude," *COURSERA: Neural networks for machine learning*, vol. 4, no. 2, pp. 26–31, 2012.

[75] L. Gatys, A. S. Ecker, and M. Bethge, "Texture synthesis using convolutional neural networks," in *Advances in neural information processing systems*, 2015, pp. 262–270.

[76] E. Hayman, B. Caputo, M. Fritz, and J.-O. Eklundh, "On the significance of real-world conditions for material classification," in *European Conference on Computer Vision*. Springer, 2004, pp. 253–266.

[77] M. Cimpoi, S. Maji, I. Kokkinos, S. Mohamed, and A. Vedaldi, "Describing textures in the wild," in *Proceedings of the IEEE Conference on Computer Vision and Pattern Recognition*, 2014, pp. 3606–3613.

[78] K. J. Dana, B. Van Ginneken, S. K. Nayar, and J. J. Koenderink, "Reflectance and texture of real-world surfaces," *ACM Transactions On Graphics (TOG)*, vol. 18, no. 1, pp. 1–34, 1999.

[79] A. Chahi, Y. Ruichek, R. Touahni *et al.*, "Local directional ternary pattern: A new texture descriptor for texture classification," *Computer Vision and Image Understanding*, vol. 169, pp. 14–27, 2018.

[80] I. El Khadiri, M. Kas, Y. El Merabet, Y. Ruichek, and R. Touahni, "Repulsive-and-attractive local binary gradient contours: New and efficient feature descriptors for texture classification," *Information Sciences*, vol. 467, pp. 634–653, 2018.

[81] Y. Ruichek *et al.*, "Local concave-and-convex micro-structure patterns for texture classification," *Pattern Recognition*, vol. 76, pp. 303–322, 2018.

[82] Y. Ruichek *et al.*, "Attractive-and-repulsive center-symmetric local binary patterns for texture classification," *Engineering Applications of Artificial Intelligence*, vol. 78, pp. 158–172, 2019.

[83] Y. Dong, T. Wang, C. Yang, L. Zheng, B. Song, L. Wang, and M. Jin, "Locally directional and extremal pattern for texture classification," *IEEE Access*, vol. 7, pp. 87 931–87 942, 2019.

[84] Y. Yang and S. Newsam, "Bag-of-visual-words and spatial extensions for land-use classification," in *Proceedings of the 18th SIGSPATIAL international conference on advances in geographic information systems*. ACM, 2010, pp. 270–279.

[85] G.-S. Xia, W. Yang, J. Delon, Y. Gousseau, H. Sun, and H. Maître, "Structural high-resolution satellite image indexing," in *ISPRS TC VII Symposium-100 Years ISPRS*, vol. 38, 2010, pp. 298–303.

[86] G.-S. Xia, J. Hu, F. Hu, B. Shi, X. Bai, Y. Zhong, L. Zhang, and X. Lu, "Aid: A benchmark data set for performance evaluation of aerial scene classification," *IEEE Transactions on Geoscience and Remote Sensing*, vol. 55, no. 7, pp. 3965–3981, 2017.

[87] Q. Zou, L. Ni, T. Zhang, and Q. Wang, "Deep learning based feature selection for remote sensing scene classification," *IEEE Geoscience and Remote Sensing Letters*, vol. 12, no. 11, pp. 2321–2325, 2015.

[88] Cheng, Gong, Han, Junwei, Lu, and Xiaoqiang, "Remote sensing image scene classification: Benchmark and state of the art," *Proceedings of the IEEE*, vol. 10, no. 105, pp. 1865–1883, 2017.

[89] K. Qi, C. Yang, Q. Guan, H. Wu, and J. Gong, "A multiscale deeply described correlatons-based model for land-use scene classification," *Remote Sensing*, vol. 9, no. 9, p. 917, 2017.

[90] K. Qi, Q. Guan, C. Yang, F. Peng, S. Shen, and H. Wu, "Concentric circle pooling in deep convolutional networks for remote sensing scene classification," *Remote Sensing*, vol. 10, no. 6, p. 934, 2018.

[91] S. Chaib, H. Liu, Y. Gu, and H. Yao, "Deep feature fusion for vhr remote sensing scene classification," *IEEE Transactions on Geoscience and Remote Sensing*, vol. 55, no. 8, pp. 4775–4784, 2017.

[92] X. Lu, H. Sun, and X. Zheng, "A feature aggregation convolutional neural network for remote sensing scene classification," *IEEE Transactions on Geoscience and Remote Sensing*, vol. 57, no. 10, pp. 7894–7906, 2019.

[93] B. Zhang, Y. Zhang, and S. Wang, "A lightweight and discriminative model for remote sensing scene classification with multidilation pooling module," *IEEE Journal of Selected Topics in Applied Earth Observations and Remote Sensing*, vol. 12, no. 8, pp. 2636–2653, 2019.

[94] R. M. Anwer, F. S. Khan, J. van de Weijer, M. Molinier, and J. Laaksonen, "Binary patterns encoded convolutional neural networks for texture recognition and remote sensing scene classification," *ISPRS journal of photogrammetry and remote sensing*, vol. 138, pp. 74–85, 2018.

[95] B. Yuan, S. Li, and L. Ning, "Multiscale deep features learning for land-use scene recognition," *Journal of Applied Remote Sensing*, vol. 12, no. 1, p. 1, 2018.

[96] G. Cheng, Z. Li, X. Yao, L. Guo, and Z. Wei, "Remote sensing image scene classification using bag of convolutional features," *IEEE Geoscience and Remote Sensing Letters*, vol. 14, no. 10, pp. 1735–1739, Oct. 2017.

[97] Y. Yu, X. Li, and F. Liu, "Attention gans: Unsupervised deep feature learning for aerial scene classification," *IEEE Transactions on Geoscience and Remote Sensing*, vol. 58, no. 1, pp. 519–531, Jan. 2020.

[98] Y. Yu and F. Liu, "Dense connectivity based two-stream deep feature fusion framework for aerial scene classification," *Remote Sensing*, vol. 10, no. 7, p. 1158, 2018.

Mengkun Liu received the B.S. and M.S. degrees from Xi'an University of Technology, Xi'an, China, in 2014 and 2017 respectively, where she is currently pursuing the Ph.D. degree in Key Laboratory of Intelligent Perception and Image Understanding of Ministry of Education, School of Artificial Intelligence Xidian University, Xi'an, China. Her research interests include machine learning and image processing.

Licheng Jiao (F'2017) received the B.S.degree from Shanghai Jiaotong University, Shanghai, China, in 1982 and the M.S. and PhD degree from Xi'an Jiaotong University, Xi'an, China, in 1984 and 1990, respectively. Since 1992, he has been a Professor with the School of Artificial Intelligence, Xidian University, Xi'an, where he is currently the Director of Key Laboratory of Intelligent Perception and Image Understanding of the Ministry of Education of China. His research interests include image processing, natural computation, machine learning, and intelligent information processing. Dr. Jiao is a member of the IEEE Xi'an Section Execution Committee, the Chairman of the Awards and Recognition Committee, the Vice Board Chairperson of the Chinese Association of Artificial Intelligence, a Councilor of the Chinese Institute of Electronics, a committee member of the Chinese Committee of Neural Networks, and an expert of the Academic Degrees Committee of the State Council. IEEE Fellow, IET Fellow, CAAI Fellow, CCF Fellow, CIE Fellow, CAA Fellow, PC of NeurIPS, ICML, CVPR, AAAI, IJCAI and ICCV.

Xu Liu (M'19) received the B.Sc. degrees in Mathematics and applied mathematics from North University of China, Taiyuan, China in 2013. He received the Ph.D. degrees from Xidian University, Xian, China, in 2019. He is also a IEEE Geoscience and Remote Sensing Society Member. He is currently a postdoctoral researcher of Key Laboratory of Intelligent Perception and Image Understanding of Ministry of Education, School of Artificial Intelligence Xidian University, Xi'an, China. His research interests include machine learning and image processing.

Lingling Li (M'17) Lingling Li received the B.S. and Ph.D. degrees from Xidian University, Xi'an, China, in 2011 and 2017 respectively. Between 2013 - 2014, she was an exchange Ph.D. student with the Intelligent Systems Group, Department of Computer Science and Artificial Intelligence, University of the Basque Country UPV/EHU, Spain. She is currently a postdoctoral researcher in the School of Artificial Intelligence at Xidian University. Her current research interests include quantum evolutionary optimization, machine learning and deep learning.

Fang Liu (SM'07) received the B.S. degree in computer science and technology from Xi'an Jiaotong University, Xi'an, China, in 1984 and the M.S. degree in computer science and technology from Xidian University, Xi'an, in 1995. She is currently a Professor with the School of Computer Science, Xidian University. Her research interests include signal and image processing, synthetic aperture radar image processing, multiscale geometry analysis, learning theory and algorithms, optimization problems, and data mining.

Shuyuan Yang (SM'14) received the B.A. degree in electrical engineering, the M.S. and Ph.D. degrees in circuit and system from Xidian University, Xian, China, in 2000, 2003, and 2005, respectively. She has been a Professor School of Artificial Intelligence Xidian University, Xi'an, China. Her research interests include machine learning and multiscale geometric analysis.